

Effect of splitter plate angular position on wake characteristics of a cylinder

Fırat Ekinci^{1*}, Engin Pinar², Tahir Durhasan³, and Huseyin Akilli⁴

¹Adana Alparslan Türkeş Science and Technology University, Engineering Faculty, Energy Systems Engineering Department, 01250 Adana, Türkiye

²Cukurova University, Ceyhan Engineering Faculty, Mechanical Engineering Department, 01950 Adana, Türkiye

³Adana Alparslan Türkeş Science and Technology University, Aeronautics and Astronautics Faculty, Aerospace Engineering Department, 01250 Adana, Türkiye

⁴Cukurova University, Engineering Faculty, Mechanical Engineering Department, 01330 Adana, Türkiye

Abstract. This study experimentally investigates the wake characteristics dynamics of a circular cylinder at $Re = 7500$ with uniform flow in a recirculating water channel, utilizing the particle image velocimetry (PIV) technique. The research examines the passive control of unsteady vortex shedding downstream of a cylinder using a splitter plate placed parallel to the cylinder surface, focusing on the effects of the oncoming flow angle and plate length. The experimental results are presented in terms of vorticity and Reynolds shear stress contours, as well as variations of maximum turbulent kinetic energy and Strouhal number with respect to the flow angle, to provide insight into the underlying fluid dynamics and vortex formation mechanisms. The gap ratio between the cylinder surface and the plate was kept constant at $g/D = 0.9$ for all cases. The oncoming flow angles were set to $\alpha = 130^\circ, 140^\circ, 150^\circ,$ and 180° , while the plate length ratios were assigned as $L/D = 0.5$ and 1 . The position and length of the splitter plate directly affect the vortex structures compared to the base cylinder case. The most effective oncoming flow angle varies with the plate length. Overall, the results indicate that splitter plates provide an effective means of flow control by suppressing vortex formation across all flow angles.

1 Introduction

Flow over bluff bodies is characterized by unstable separation and periodic vortex shedding, resulting in variable hydrodynamic forces and broadband acoustic emissions. In engineering systems such as offshore risers, heat exchanger tubes, bridge cables, and chimneys, these unstable stresses result in vortex-induced vibration (VIV), affecting structural integrity, fatigue life, and serviceability. The circular cylinder effectively embodies the fundamental physics of bluff-body wakes while being empirically practicable; hence, it has historically functioned as a reference model for examining shedding dynamics and formulating flow-control measures.

There are two main types of flow control strategies for reducing shedding and vortex-induced vibrations: active and passive. Active methods use outside energy sources, like synthetic jets or plasma actuation, to control shear layer instabilities. This gives you control, but it also makes things more complicated. In contrast, passive control alters the topology of the near and far wake regions through geometric modifications, such as surface treatments, auxiliary bodies, or appendages, without the need for external power. The simplicity and durability of passive control methods render them

appealing for field implementation in energy, maritime, and civil applications.

Installing a control plate, also known as a splitter plate, downstream of the cylinder is an effective passive control strategy, as it directly addresses the momentum deficit and the large-scale coherence of the separated wake. A splitter plate can inhibit or attenuate the interaction of counter-rotating shear layers, so suppress the instability that leads to Karman vortex formation. Reported advantages include reduced mean drag, diminished lift fluctuation, and a shorter spectral peak at the Strouhal shedding frequency [1–3]. Simultaneously, using a plate with improper placement may introduce extraneous vortex modes or enhance three-dimensionality [4–6].

Previous studies have shown that splitter plates are investigated experimentally and numerically to comprehend the flow characteristic evaluation of the plate's intrusion in the wake region of bluff bodies. Due to the increase in the base pressure of the cylinder, splitter plates provide to suppress vortex shedding formation [7,8]. Furthermore, splitter plates positioned behind the body has been effectively employed to suppress vortex structures and to reduce the Strouhal (St) number at both low [9–11] and high Reynolds (Re) numbers [12–16]. Besides, flexible and rigid splitter plates have been conducted to observe the flow

* Corresponding author: fekinci@atu.edu.tr

characteristics [17,18]. For instance, Sharma et al. [19] examined the effects of rigid and flexible splitter plates positioned behind a square-section cylinder on flow regulation at Reynolds numbers of 600, 1000, and 2000. The researchers examined the impact of splitter plate length and its flexibility on flow shape and forces. The results demonstrate that the length of the splitter plate independently influences flow frequency, and the average drag coefficient. Flexible plates demonstrated superior efficacy compared to rigid plates, especially at elevated Reynolds numbers, emphasizing their importance in passive flow regulation within intermediate regimes. In addition to the attached and detached configurations behind of the bluff body, splitter plate can also be used as guide vanes to manipulate the flow around the bluff body [20,21].

However, splitter plates are rarely positioned such that the ray emanating from the center of the cylinder is perpendicular to the plate in the literature. Therefore, the aim of the present study is to experimentally investigate a splitter plate arranged parallel to the cylinder surface, with two different plate lengths and various angular positions relative to the cylinder's origin. The experiments were conducted at the Reynolds number of $Re = 7500$, based on the cylinder diameter (D). The gap ratio (g) between the cylinder surface and the plate was kept constant at $g/D = 0.9$ for all cases. The oncoming flow angles were set to $\alpha = 130^\circ, 140^\circ, 150^\circ, \text{ and } 180^\circ$, while the plate length ratios were assigned as $L/D = 0.5$ and 1 . The wake flow characteristics are thoroughly examined to clarify the influence of plate configuration on the vortex dynamics.

2 Experimental method

All experiments were conducted in a closed-circuit recirculating water channel featuring a free surface, fabricated from 15 mm transparent plexiglas for optical access at the Department of Mechanical Engineering, Cukurova University, utilizing a base circular cylinder (outer diameter, $D = 50 \pm 0.05$ mm) and solid splitter plates (thickness, $T = 5 \pm 0.05$ mm). The channel features a Plexiglas test area measuring 8,000 mm in length, 1,000 mm in width, and 750 mm in height, ensuring optimal visibility for particle image velocimetry (PIV) measurements. A speed control unit enabled the user to adjust the frequency of a 15 kW centrifugal pump, thereby regulating the free stream velocity. With free-stream turbulence predicted to be less than 1%, honeycomb configurations were positioned inside the channel to further reduce it. The channel has free-stream turbulence intensity of less than 1.5%. Based on the cylinder's diameter, the free stream velocity was determined to be $140 \text{ mm/s} \pm 3\%$, giving a Reynolds number of $Re = 7500 \pm 4\%$ based on the cylinder diameter. The water temperature was maintained at $23 \pm 1^\circ\text{C}$ using a cooling system. The overall water depth in the channel was maintained at $500 \text{ mm} \pm 2$ during every experiment. Two important parameters that were examined in this study are oncoming flow angle, $\alpha = 130^\circ, 140^\circ, 150^\circ, \text{ and } 180^\circ$, and the length of the parallel plates (i.e., nondimensionalized plate length ratio, L/D

$= 0.5$ and 1), respectively. This passive approach would likely be unusable in the field if the length increased above $1D$. The ratio of the shortest gap between the parallel plates and the cylinder to the cylinder diameter (gap ratio, $g/D = 0.9$) was kept constant. Figure 1a shows the reference coordinate system and cross-sections of the cylinder with parallel plates for length ratio, L/D ratios of 0.5 and 1 , as well as a gap ratio, g/D ratio of 0.9 .

Figure 1b presents the schematically PIV setup and corresponding cylinder configuration. An end plate was rigidly attached to the channel bottom using double-sided tape. The center of the end plate intersects the longitudinal line passing through the center (mid-width) of the channel. The end plates and the cylinder are mounted tightly (interference fit). Parallel plates were connected by end plates to the cylinder. A rod was used to keep the cylinder in a vertical position. The maximum blockage encountered in the experiments was 6%. The effective aspect ratio of the system consisting of a cylinder and a double parallel plate was 8%. Subsequently, two-component planar particle image velocimetry (PIV) observations were conducted in the x - y plane. The origin of the x - y plane was designated as the middle of the cylinder. Two-component planar particle image velocimetry (PIV) observations were conducted in the x - y plane. The origin of the x - y plane was designated as the middle of the cylinder. Subsequently, the measurements were conducted, and the results were analyzed utilizing the Dantec Dynamics PIV system and Flow Manager Software on a computer. The measurement field was illuminated by a thin and intense laser light sheet using a pair of double-pulsed Nd:YAG laser units, each with a maximum energy output of 120 mJ at 532 nm wavelength. The image pairs were captured by a Dantec Dynamics, FlowSense 2M CCD camera, which has a pixel resolution of 1600×1200 and a bit depth of 10. The x - y plane field of vision (FOV) was approximately $216.4 \text{ mm} \times 162.3 \text{ mm}$ ($4.33D \times 3.25D$) thanks to the 60 mm lens on the camera (Nikon, AF Micro-Nikkon 60mm $f/2.8D$). A grid size of $2.16 \text{ mm} \times 2.16 \text{ mm}$ ($0.043D \times 0.043D$) was used effectively. For all tests, the pulse interval was 1.5 ms, and the measurement plane was illuminated by a laser sheet that was about 2 mm thick. To achieve the highest possible particle displacement inside the interrogation window, the time interval and laser sheet thickness were optimized as previously achieved in the literature [22,23].

The velocity uncertainty in the current experiment is approximately 2%. Silver-coated hollow glass spheres with an average diameter of $10 \mu\text{m}$ and a density of 1.4 g/cm^3 were employed to seed the flow. In every experiment, 1000 instantaneous pictures were collected at a frequency of 15 Hz, analysed, and stored to derive time-averaged velocity vectors [24]. Finally, the subsequent processing yielded the instantaneous and mean vorticity maps, turbulence statistics, and the vorticity value at each grid point.

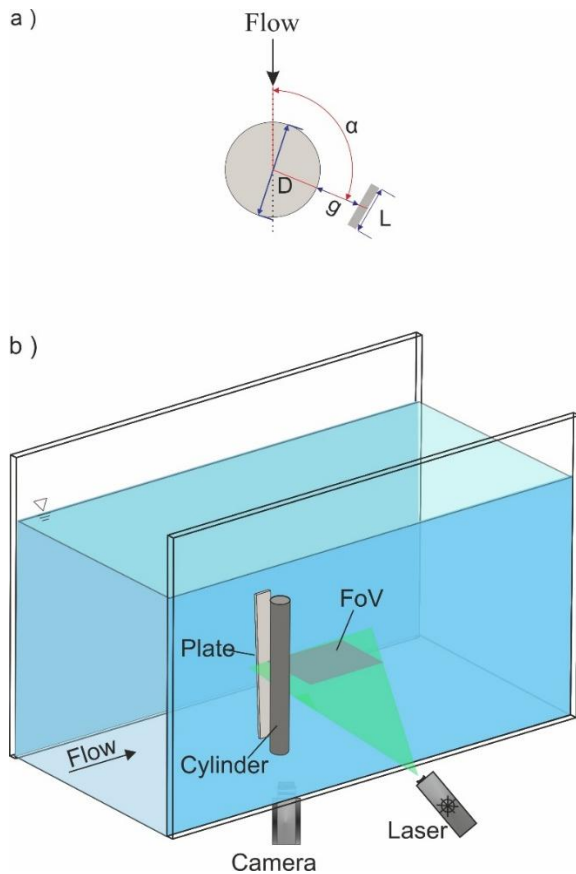


Fig. 1. Experimental setup a) schematic representation of cylinder configuration, b) overall view of PIV setup.

3 Results and discussion

In this study, the effects of a splitter plate placed in the near wake of a circular cylinder were investigated for a fixed gap ratio of $g/D = 0.9$ at four different oncoming flow angles: $\alpha = \pm 130^\circ, 140^\circ, 150^\circ,$ and 180° . The primary objective of the study was to prevent or eliminate unstable vortices that could affect the cylinder.

Therefore, the flow characteristics behind the base cylinder were investigated as a reference case. Figure 2 shows the time-averaged flow patterns of vorticity $|\omega|$ and the time-averaged flow patterns of Reynolds stress correlations $|u'v'/U^2|$ for a base circular cylinder, respectively. The blue and pink lines present positive and negative contours, respectively. The minimum and incremental values of time averaged vorticity, $|\omega|$ contours were taken as ± 5 and 5, respectively.

The time-averaged vorticity contours in the near wake region of the base cylinder exhibits a uniform and symmetrical flow structure, converging in proximity within the wake region. In the no-plate (uncontrolled) configuration, the time-averaged flow field has transformed the periodic Karman shedding into a steady, symmetric wake. The wake is defined by a closed recirculation region immediately downstream of the cylinder. The free shear layers expand and move downstream, characterizing the bubble as a region of negative and positive streamwise velocity, consistent with the separation at the cylinder's lateral surfaces. The mean vorticity field displays peak magnitudes corresponding to these shear layers; however, at the

centerline, the opposing contributions from both sides partially negate each other, resulting in a low-vorticity corridor in which the deficit progressively recovers. This basic topology provides a quantitative benchmark to evaluate how a plate positioned in the near wake region, dominated by the recirculation zone and shear layer, would alter separation, affect bubble length, and reduce unsteady vortices within the near wake.

The minimum and incremental values of Reynolds shear stress, $|u'v'/U^2|$ contours, were taken as ± 0.01 and 0.01, respectively. Four clusters of Reynolds shear stress contours are seen, with two exhibiting positive values and the other two negative values. However, a pair of clusters of Reynolds shear stress contours with diminished intensity is observed in the recirculating flow region of the base cylinder. The figure illustrates that the contours of negative and positive Reynolds shear stress, $|u'v'/U^2|$, exhibit symmetry along the cylinder's centerline. This fundamental distribution serves as the benchmark from which we anticipate a reduction in stresses and a displacement of the peaks when a plate is incorporated. Once the shear layers detach from the cylinder shoulders, turbulence generation escalates, and the time-averaged Reynolds shear stress attains its peak values in these layers.

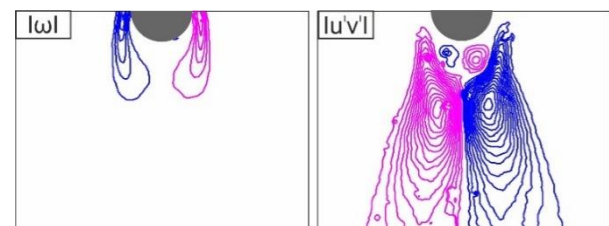


Fig. 2. Patterns of time-averaged vorticity contours ($|\omega|$) and Reynolds stress contours ($|u'v'|$) at the downstream of base cylinders.

Figure 3 shows the contours of time-averaged vorticity ($|\omega|$) presented for oncoming flow angles $\alpha = 130^\circ, 140^\circ, 150^\circ,$ and 180° , with a splitter plate positioned in the cylinder's wake region. The first column displays the flow structures for a length ratio of $L/D = 0.5$, while the second column presents the flow structures for the length ratio of $L/D = 1$.

For all cases except the oncoming flow angle at $\alpha = 180^\circ$, the flow separated from both the circular cylinder and the splitter plate, causing the formation of two sets of positive and negative vortices in the near wake of the circular cylinder. Also, the flow separated from both the circular cylinder and the splitter plate generates two sets of positive and negative vortices in the near wake region. Nonetheless, when the splitter plate is employed, the length of the vortex generated by the circular cylinder is longer than that of the base cylinder in all instances. The jet flow passing through the cylinder and the splitter plate is oriented towards the circular cylinder. Consequently, the wake of the circular cylinder constricts with an increasing flow incidence angle, but the wake of the splitter plate progressively expands.

For oncoming flow angles of $\alpha = 130^\circ, 140^\circ,$ and 150° , the vortices generated by the splitter plate are elongated in the case with a length ratio of $L/D = 1$

compared to the scenario with a length ratio of $L/D = 0.5$.

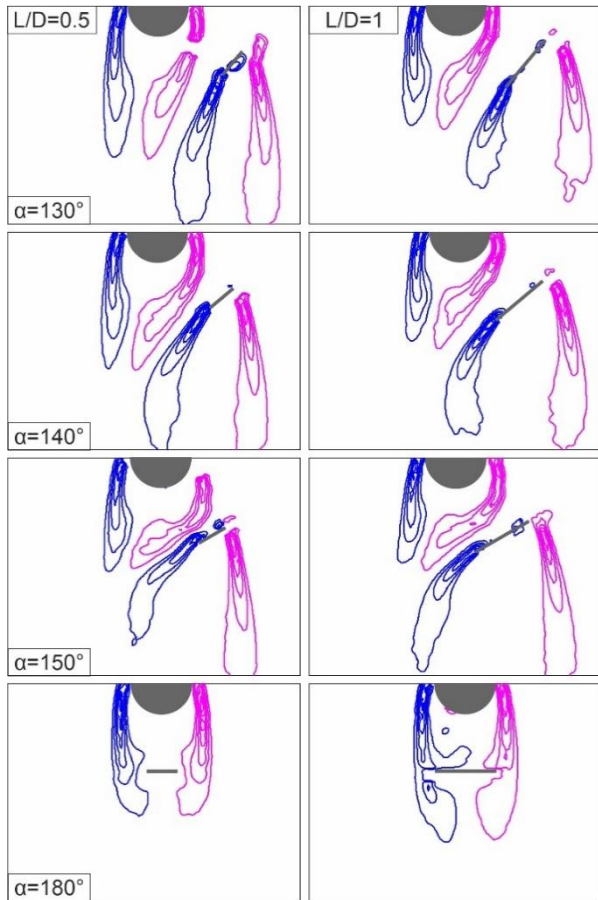


Fig. 3. Patterns of time-averaged vorticity contours (ω) for splitter plate configurations.

Figure 4 illustrates the time-averaged correlations of the Reynolds shear stress ($u'v'$) contours for oncoming flow angles $\alpha = 130^\circ, 140^\circ, 150^\circ,$ and 180° , with a splitter plate positioned in the cylinder's wake region, which remains inadequately detailed. The flow structures for a length ratio of $L/D = 0.5$ are presented in the first column, while those for a length ratio of $L/D = 1$ are displayed in the second column.

When the flow structures consisting of a circular cylinder and a splitter plate pair are examined for all oncoming flow angles, there are high turbulence intensities, and as a result, a complex flow structure is formed. At oncoming flow angles of $\alpha = 130^\circ, 140^\circ,$ and 150° , two distinct wakes are generated in the flow field, which are separate but interact with one another, in contrast to the case involving just one base cylinder. At a flow angle of $\alpha = 180^\circ$, the flow structure, comprising a circular cylinder and a splitter plate, generates a singular wake, analogous to the scenario with only a base cylinder in the flow field.

The magnitudes of the Reynolds shear stress in the wake of both the circular cylinder and the splitter plate decreased compared to the base cylinder case across all flow angles and for both length ratios. The installation of the splitter plate in the wake of the circular cylinder significantly diminishes turbulence statistics. Unless the oncoming flow angle is $\alpha = 180^\circ$, the jet flow passing between the cylinder and the splitter plate pair is

directed towards the circular cylinder. As a result, the wake created by the circular cylinder narrows, and the wake created by the splitter plate expands.

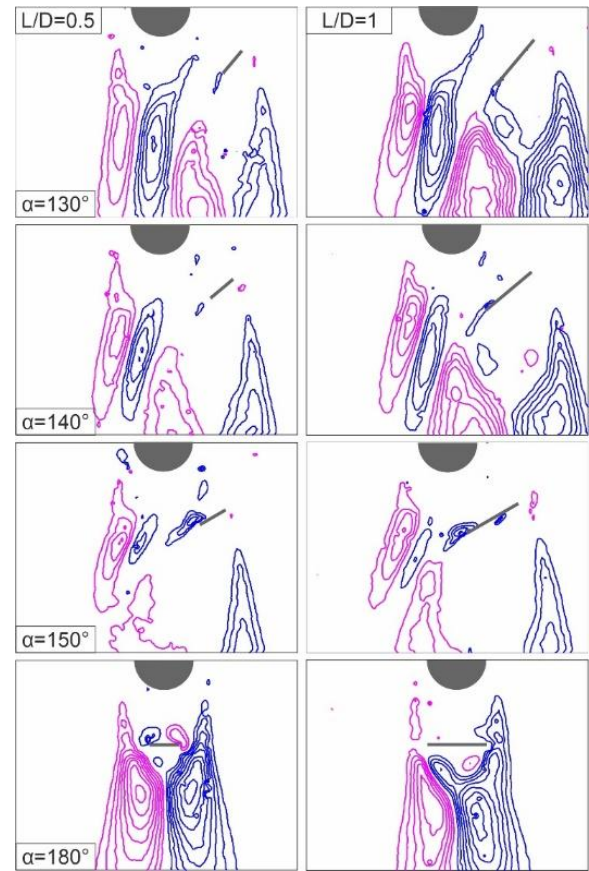


Fig. 4. Patterns of time-averaged Reynolds stress contours ($u'v'$) for splitter plate configurations.

Figure 5 illustrates the variation of the maximum turbulent kinetic energy (TKE) value in relation to the oncoming flow angle for both length ratios of the plate. The highest TKE value recorded without a splitter plate as a control mechanism at the wake region of a base cylinder was found to be 0.45. The graph indicates that the inclusion of a splitter plate as a control element in the wake region of a base cylinder significantly diminishes turbulence statistics in the vicinity of the circular cylinder at all oncoming flow angles. However, the most effective oncoming flow angle is $\alpha = 140^\circ$ when the length ratio (L/D) is 0.5, and $\alpha = 150^\circ$ when the length ratio (L/D) is 0.1. The lowest maximum TKE values were determined to be 0.126 and 0.107 for length ratio, $L/D = 0.5$ and 1, respectively. After the oncoming flow angle values of $\alpha = 140^\circ$ and 150° , the maximum TKE value increases with increasing flow angle. However, the highest values obtained are still lower than the maximum TKE value obtained when only base cylinder is used.

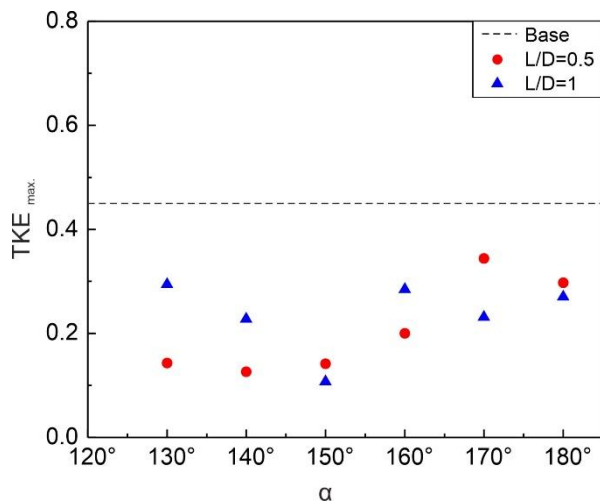


Fig. 5. The variation of TKE_{max} with respect α variation for both plate lengths.

Figure 6 provides the variation of Strouhal (St) number with respect oncoming flow angles. Vortex shedding frequencies are determined for cylinder wake and plate wake. In this context, Strouhal numbers are calculated separately based on the characteristic lengths of the cylinder and plate. The horizontal dashed line represents the baseline St value ($=0.21$) for the base cylinder configuration without any flow control device. The implementation of splitter plates consistently modifies the vortex shedding characteristics across all tested angles, as evidenced by the deviation of St values from the baseline case. For the shorter splitter plate configuration ($L/D = 0.5$), the St_c values exhibit a notable increase above the baseline, indicating an intensification of vortex shedding frequency of the cylinder especially for $\alpha \leq 150^\circ$. The St_p value of the plate gradually diminishes up to $\alpha = 150^\circ$, and beyond this angle, St_p cannot be determined because the cylinder dominates the formation wake flow structure. St_c values get close the baseline cylinder for $\alpha > 150^\circ$.

The longer splitter plate configuration ($L/D = 1$) demonstrates more effective on the vortex shedding process. passive flow control characteristics. St_c value remarkably increase in comparison with the baseline cylinder for $\alpha \leq 160^\circ$. Furthermore, St_p values are higher than that obtained from $L/D=0.5$. However, the suppression of St_c , particularly evident at $\alpha=170^\circ$ and 180° , indicates a stabilization of the near-wake region and a reduction in vortex shedding intensity. The angular dependency of St_c reveals that the effectiveness of the splitter plate is strongly influenced by its orientation relative to the oncoming flow.

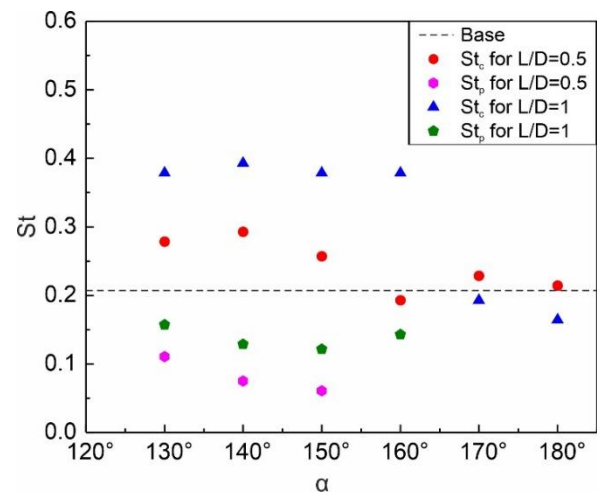


Fig. 6. The variation of St with respect α variation for both plate lengths.

4 Conclusion

This study experimentally investigated the passive flow control characteristics of a splitter plate mounted parallel to the cylinder surface submerged in deep water. The research systematically quantified the influence of plate length ratio ($L/D = 0.5$ and 1) and oncoming flow angle ($\alpha = 130^\circ, 140^\circ, 150^\circ$, and 180°) on wake dynamics and turbulence characteristics at a fixed gap ratio of $g/D = 0.9$.

The experimental results reveal substantial modifications to the wake structure induced by the splitter plate configuration. Key findings include: (i) significant attenuation of large-scale Karman vortex shedding, (ii) reconfiguration and elongation of the recirculation zone, (iii) marked reductions in turbulent kinetic energy (TKE) and Reynolds shear stress magnitudes, and (iv) downstream displacement of the peak stress location. These observations collectively demonstrate the efficacy of splitter plates as passive flow control devices for mitigating wake-induced instabilities in cylindrical structures. The optimal flow oncoming angles are $\alpha = 140^\circ$ for a length ratio of $L/D = 0.5$ and $\alpha = 150^\circ$ for a length ratio of $L/D = 1$. The longer splitter plate configuration ($L/D = 1$) achieved higher turbulence suppression, with minimum peak TKE values of 0.126 and 0.107 for $L/D = 0.5$ and $L/D = 1$, respectively, representing significant reductions compared to the baseline cylinder configuration.

These findings validate the potential of splitter plates as practical and cost-effective passive flow control devices for engineering applications involving circular cylinders.

References

1. M. Matsumoto, Vortex Shedding Of Bluff Bodies: A Review. *J. Fluids Struct.* **13**, 791 (1999). <https://www.doi.org/10.1006/jfls.1999.0249>
2. E. Rathakrishnan, Effect of Splitter Plate on Bluff Body Drag. *AIAA J.* **37**, 1125 (1999). <https://doi.org/10.2514/2.823>

3. H. Choi, W.-P. Jeon, and J. Kim, Control of Flow Over a Bluff Body. *Annu. Rev. Fluid Mech.* **40**, 113 (2008).
<https://doi.org/10.1146/annurev.fluid.39.050905.110149>
4. M. M. Zdravkovich, Review and classification of various aerodynamic and hydrodynamic means for suppressing vortex shedding. *J. Wind Eng. Ind. Aerodyn.* **7**, 145 (1981). [https://doi.org/10.1016/0167-6105\(81\)90036-2](https://doi.org/10.1016/0167-6105(81)90036-2)
5. J. F. Derakhshandeh and M. M. Alam, A review of bluff body wakes. *Ocean Eng.* **182**, 475 (2019).
<https://doi.org/10.1016/j.oceaneng.2019.04.093>
6. M. Zhao, A review of recent studies on the control of vortex-induced vibration of circular cylinders. *Ocean Eng.* **285**, 115389 (2023).
<https://doi.org/10.1016/j.oceaneng.2023.115389>
7. A. Roshko, On the Wake and Drag of Bluff Bodies. *J. Aeronaut. Sci.* **22**, 124 (1955).
<https://doi.org/10.2514/8.3286>
8. C. J. Apelt, G. S. West, and A. A. Szewczyk, The effects of wake splitter plates on the flow past a circular cylinder in the range $10^4 < R < 5 \times 10^4$. *J. Fluid Mech.* **61**, 187 (1973).
<https://doi.org/10.1017/S0022112073000649>
9. M. S. Mat Ali, C. J. Doolan, and V. Wheatley, Low Reynolds number flow over a square cylinder with a splitter plate. *Phys. Fluids* **23**, 033602 (2011).
<https://doi.org/10.1063/1.3563619>
10. H. C. Vu, J. Ahn, and J. H. Hwang, Numerical investigation of flow around circular cylinder with splitter plate. *KSCE J. Civ. Eng.* **20**, 2559 (2016).
<https://doi.org/10.1007/s12205-015-0209-3>
11. H. C. Onel, T. Durhasan, M. M. Aksoy, and İ. Karasu, Wake flow characteristics of diamond-shaped cylinder with splitter plate. *Ocean Eng.* **326**, 120933 (2025).
<https://doi.org/10.1016/j.oceaneng.2025.120933>
12. E. A. Anderson and A. A. Szewczyk, Effects of a splitter plate on the near wake of a circular cylinder in 2 and 3-dimensional flow configurations. *Exp. Fluids* **23**, 161 (1997). <https://doi.org/10.1007/s003480050098>
13. G. R. S. Assi, P. W. Bearman, and N. Kitney, Low drag solutions for suppressing vortex-induced vibration of circular cylinders. *J. Fluids Struct.* **25**, 666 (2009).
<https://doi.org/10.1016/j.jfluidstructs.2008.11.002>
14. F. Gu, J. S. Wang, X. Q. Qiao, and Z. Huang, Pressure distribution, fluctuating forces and vortex shedding behavior of circular cylinder with rotatable splitter plates. *J. Fluids Struct.* **28**, 263 (2012).
<https://doi.org/10.1016/j.jfluidstructs.2011.11.005>
15. K. Liu, J. Deng, and M. Mei, Experimental study on the confined flow over a circular cylinder with a splitter plate. *Flow Meas. Instrum.* **51**, 95 (2016).
<https://doi.org/10.1016/j.flowmeasinst.2016.09.002>
16. J. Zhou, X. Qiu, J. Li, B. Wang, Q. Zhou, and Y. Liu, The experimental investigation on wake dynamics of flow around a circular cylinder with the splitter plate. *J. Fluids Struct.* **127**, 104130 (2024).
<https://doi.org/10.1016/j.jfluidstructs.2024.104130>
17. S. Shukla, R. N. Govardhan, and J. H. Arakeri, Flow over a circular cylinder with a flexible splitter plate. *J. Fluid Mech.* **973**, A19 (2023).
<https://doi.org/10.1017/jfm.2023.755>
18. T. R. Sahu, M. Furquan, Y. Jaiswal, and S. Mittal, Flow-induced vibration of a circular cylinder with rigid splitter plate. *J. Fluids Struct.* **89**, 244 (2019).
<https://doi.org/10.1016/j.jfluidstructs.2019.03.015>
19. K. R. Sharma and S. Dutta, Flow control over a square cylinder using attached rigid and flexible splitter plate at intermediate flow regime. *Phys. Fluids* **32**, 014104 (2020). <https://doi.org/10.1063/1.5127905>
20. F. Ekinçi, T. Durhasan, and H. Akilli, Silindir Art İzindeki Daimi Olmayan Girdapların Kılavuz Plakalar Yardımı ile Bastırılması. *Çukurova Üniversitesi Mühendis. Fakültesi Derg.* **38**, 593 (2023).
<https://doi.org/10.21605/cukurovaumfd.1377170>
21. T. Durhasan, F. Ekinçi, E. Firat, and H. Akilli, An experimental investigation of the flow control of a circular cylinder in near wake with parallel plates at $Re = 7500$. *Int. J. Heat Fluid Flow* **106**, 109276 (2024).
<https://doi.org/10.1016/j.ijheatfluidflow.2024.109276>
22. M. M. Aksoy, Experimental investigation of wake flow characteristics of slotted hollow circular cylinder. *Ocean Eng.* **341**, 122584 (2025).
<https://doi.org/10.1016/j.oceaneng.2025.122584>
23. T. Durhasan, E. Pinar, G. M. Ozkan, M. M. Aksoy, H. Akilli, and B. Sahin, PIV measurement downstream of perforated cylinder in deep water. *Eur. J. Mech. - BFluids* **72**, 225 (2018).
<https://doi.org/10.1016/j.euromechflu.2018.06.001>
24. E. Pinar, G. M. Ozkan, T. Durhasan, M. M. Aksoy, H. Akilli, and B. Sahin, Flow structure around perforated cylinders in shallow water. *J. Fluids Struct.* **55**, 52 (2015).
<https://doi.org/10.1016/j.jfluidstructs.2015.01.017>